Journal of Power Sources 213 (2012) 338–342

Contents lists available at SciVerse ScienceDirect

Journal of Power Sources

journal homepage: www.elsevier.com/locate/jpowsour

Short communication

Nickel ferrite–graphene heteroarchitectures: Toward high-performance anode materials for lithium-ion batteries

Yongsheng Fu [a], Yunhai Wan [b], Hui Xia [a,b,**], Xin Wang [a,*]

[a] Key Laboratory of Soft Chemistry and Functional Materials, Nanjing University of Science and Technology, Ministry of Education, Nanjing 210094, China
[b] School of Materials Science and Engineering, Nanjing University of Science and Technology, Nanjing 210094, China

ARTICLE INFO

Article history:
Received 28 January 2012
Received in revised form
16 April 2012
Accepted 19 April 2012
Available online 26 April 2012

Keywords:
Nickel ferrite
Graphene
Lithium-ion batteries
Heteroarchitecture

ABSTRACT

A $NiFe_2O_4$–graphene heteroarchitecture with differing graphene content is prepared by a straightforward hydrothermal strategy. The $NiFe_2O_4$–graphene (with 20 wt% graphene) nanocomposite as the anode material for lithium-ion batteries shows a high specific reversible capacity up to 960 mAh g^{-1} with good cycling stability and rate capability. The superior electrochemical performance of the $NiFe_2O_4$–graphene nanocomposite can be attributed to its unique heteroarchitecture, which enables high utilization of active material, good structural stability and fast charge transport.

1. Introduction

Since the first commercial lithium-ion batteries (LIBs) appeared in the early 1990s, continual improvements have made the technology more economical and popular on several accounts. Anode is one of the key components of LIBs technology and nanostructured metal oxides are the possible next-generation anode materials for high-energy LIBs due to their high capacity and wide abundance [1,2]. So far, much attention has been paid to simple metal oxides [1–5]. Among these oxides, Fe_2O_3 has been systematically studied as an anode material for LIBs due to its fascinating properties such as the high theoretical capacity (1007 mAh g^{-1}), low cost and low environmental impact [6,7]. However, large volume changes usually occur in the host matrix of Fe_2O_3 during the charging and discharging processes, resulting in pulverization and exfoliation of active material from current collector, consequently leading to capacity fading and poor cycling life. Another transition metal oxide, NiO also shows the high theoretical capacity up to 718 mAh g^{-1} and has been regarded as one of the promising anodes for LIBs. Unfortunately, although a variety of NiO materials have been tested in LIBs, none of them offered excellent long-term stability and high rate performance as anode material for high power LIBs [8–10].

It is well known that Fe_2O_3 can react with divalent metal oxides MO to form spinel MFe_2O_4. Spinel transition metal oxides (AB_2O_4) with two metal elements provide the feasibility to tune the energy density and working voltage by varying the metal content [11,12]. The initial discharge capacities of these mixed metal oxides usually exceed 900 mAh g^{-1}. Therefore, the energy density of LIBs can be promoted by using the spinel oxides as anode materials. For example, it has been reported that $NiFe_2O_4$ has been applied as anode materials for LIBs [13–15].

There have been many efforts to improve the performance of anode materials in LIBs. An effective approach is attaching metal oxide nanoparticles to carbon substrates. Conceptually, metal oxide/carbon composites are expected to be advanced electrode materials, due to the combination of electrochemical functionality of metal oxides and electrical conductivity of carbon. As a novel two-dimensional carbon material, graphene possesses good conductivity, good flexibility and high surface area, and therefore it can be used as a promising anode material in LIBs [11,12]. Several groups reported metal oxides/graphene nanocomposites as high-performance anode materials for LIBs. The lithium storage mechanism for transition metal oxide nanoparticles is referred to as a conversion mechanism, involving the formation and

* Corresponding author. Tel.: +86 25 84305667; fax: +86 25 8431 5054.
** Corresponding author. School of Materials Science and Engineering, Nanjing University of Science and Technology, Nanjing 210094, China.
E-mail addresses: jasonxiahui@gmail.com (H. Xia), wxin@public1.ptt.js.cn (X. Wang).

0378-7753/$ – see front matter © 2012 Elsevier B.V. All rights reserved.
doi:10.1016/j.jpowsour.2012.04.039

decomposition of Li_2O, accompanying the reduction and oxidation of metal nanoparticles, respectively [1]. In addition to the conversion mechanism, the extra lithium storage can occur at the surface of metal oxide nanoparticles or graphene sheets by an interfacial lithium storage mechanism or polymeric gel-like film formation mechanism [16–18].

Recently we reported a magnetically separable $NiFe_2O_4$–graphene photocatalyst and its high performance in the photocatalytic degradation of MB under visible light irradiation [19]. Herein, for the first time we demonstrate a $NiFe_2O_4$–graphene heteroarchitecture as an advanced anode material for high performance LIBs. The experimental results show that the graphene sheets in this heteroarchitectures are exfoliated and well decorated by $NiFe_2O_4$ nanocrystallines having an average diameter of 6.5 nm. It is found that the $NiFe_2O_4$–graphene nanocomposite exhibits significantly improved cycling stability and rate capability compared with the pure $NiFe_2O_4$ nanoparticles.

2. Experimental section

2.1. Synthesis of $NiFe_2O_4$–graphene heteroarchitecture

The preparation of $NiFe_2O_4$–graphene heteroarchitecture is described in detail in our previous publication [19]. The following is a brief description of the preparation: 26 mg of GO was dispersed into 70 mL of ethanol with sonication for 1 h. Then 0.291 g of $Ni(NO_3)_2 \cdot 6H_2O$ and 0.808 g of $Fe(NO_3)_3 \cdot 9H_2O$ were added into the GO dispersion solution with stirring for 30 min at room temperature. The above-mentioned solution was adjusted to a pH value of 10.0 with 6 M NaOH solution, and stirred for 30 min. The resulting mixture was transferred into a 100 mL Teflon-lined stainless steel autoclave and heated to 180 °C for 20 h under autogenous pressure. The precipitate was filtered, washed and dried. For convenient, $NiFe_2O_4$–G(0.1) is used to represent $NiFe_2O_4$–graphene nanocomposite with 10 wt% graphene and other nanocomposites with differing graphene content are expressed in the same way. All materials were characterized by Powder X-ray diffraction, transmission electron microscopy, field-emission scanning electron microscopy, nitrogen adsorption–desorption isotherms, Raman spectroscopy and X-ray photoelectron spectroscopy, and part of results were published in our previous publication [19]. Briefly, the as-obtained $NiFe_2O_4$–graphene heteroarchitecture can be indexed to a pure spinel-type $NiFe_2O_4$ (JCPDS 54-0964). Graphene oxide has been reduced to graphene with a tiny amount of residual oxygen-containing groups via hydrothermal reaction, as confirmed by XPS and Raman results. $NiFe_2O_4$–G(0.2) possess much larger BET special surface area (164.25 $m^2 g^{-1}$) compared to that of the reduced graphene oxide (35.21 $m^2 g^{-1}$) or pure $NiFe_2O_4$ (55.70 $m^2 g^{-1}$). The high special surface area of $NiFe_2O_4$–G(0.2) is attributed to the high dispersion of the $NiFe_2O_4$ nanoparticles anchored on the graphene sheets and the exfoliation of graphene sheets due to the crystal growth of $NiFe_2O_4$ between the interlayer of graphene oxide.

2.2. Electrochemical measurements

The electrode slurries were prepared by mixing 80 wt% active material (reduced graphene oxide, $NiFe_2O_4$, $NiFe_2O_4$–G(0.1), or $NiFe_2O_4$–G(0.2)), with 10 wt% acetylene black (Super-P), and 10 wt% polyvinylidene fluoride (PVDF) binder in *N*-methyl-2-pyrrolidinone (NMP). The slurries were coated on the Cu foils and dried at 120 °C for 2 h to remove the solvent. Then the dried Cu foils with electrode materials were pressed then cut into small disks (10 mm in diameter). The small disks were further dried at 80 °C in vacuum oven for 12 h before battery tests. Half cells using Li foil as both counter and reference electrodes were assembled with Lab-made Swagelok cells for electrochemical measurements. The 1 M $LiPF_6$ dissolved in the co-solvents of ethylene carbonate and diethyl carbonate (EC/DEC, v/v = 1:1) was used as the electrolyte, and the Celgard 2400 porous membrane was used as the separator. Galvanostatic charge and discharge measurements were carried out in the voltage range between 0.01 and 3.0 V at different current densities using LAND CT2001A electrochemical workstation at room temperature. Cyclic voltammograms (CVs) measurements were carried out using a CHI 660B electrochemical workstation over the potential range 0.01–3.0 V versus Li/Li^+ at a scanning rate of 1 mV s^{-1}.

3. Results and discussion

The morphologies of as-obtained $NiFe_2O_4$–graphene heteroarchitecture and pure $NiFe_2O_4$ were investigated by TEM and FESEM. As can be seen from Fig. 1A, for the pure $NiFe_2O_4$, only the aggregates of $NiFe_2O_4$ nanoparticles were obtained. For the $NiFe_2O_4$–G(0.2) heteroarchitecture, it is clearly seen that that the two-dimensional and almost transparent graphene sheets are fully exfoliated and well decorated with $NiFe_2O_4$ nanocrystals having an average diameter of 6.5 nm (Fig. 1C and D). However, for $NiFe_2O_4$–G(0.1), the aggregation of $NiFe_2O_4$ nanoparticles can be found outside the graphene sheets due to the low content of graphene (Fig. 1B). The lattice fringes with d-spacing of 0.25 nm may be assigned to the (311) plane of the cubic $NiFe_2O_4$, which is consistent with the XRD results.

Fig. 2 presents a comparison of electrochemical performances of pure $NiFe_2O_4$, reduced graphene oxide, $NiFe_2O_4$–G(0.1), and $NiFe_2O_4$–G(0.2) electrodes. Fig. 2A shows the charge/discharge curves of the pure $NiFe_2O_4$ electrode at the 1st, 2nd, 10th, 25th, and 50th cycles. In the first discharge, a voltage quasi-plateau around 0.8 V can be observed, corresponding to the transition metal reduction during Li intercalation [15,16]. In the first charge, a quasi-plateau around 1.5 V can be seen, corresponding to the transition metal oxidation [15,16]. The specific capacities of the first discharge and charge of the pure $NiFe_2O_4$ electrode are 1266 and 822 mAh g^{-1}, respectively, with an initial coulombic efficiency of 64.9%. After the first cycle, charge and discharge curves are quite symmetric with improved coulombic efficiency, but the lost capacity is significant. This electrochemical behavior is in good agreement with literature reports [14,15]. As shown in Fig. 2C and D, the charge/discharge curves of $NiFe_2O_4$–G(0.1) and $NiFe_2O_4$–G(0.2) electrodes exhibit similar behavior as the pure $NiFe_2O_4$ electrode except for the capacity losses during cycling. The discharge and charge capacities of $NiFe_2O_4$–G(0.1) for the first cycle are 1350 and 916 mAh g^{-1}, respectively, with a coulombic efficiency of 67.8%. While the discharge and charge capacities of $NiFe_2O_4$–G(0.2) for the first cycle are 1363 and 960 mAh g^{-1}, respectively, with a coulombic efficiency of 70.4%. Compared with the first cycle discharge curve of the pure $NiFe_2O_4$ electrode, the first discharge curves of the $NiFe_2O_4$–G(0.1) and $NiFe_2O_4$–G(0.2) electrodes show comparatively shorter voltage plateaus (Fig. 1C and D). It is speculated that the difference in the structural features between the pure $NiFe_2O_4$ nanoparticles and the $NiFe_2O_4$–graphene heteroarchitecture may result in differences in charge/discharge behaviors. When lithium-ions are mainly stored on the surface of the electrode material due to the interfacial mechanism, the charge/discharge curves could exhibit a sloppy profile rather than a flat voltage plateau, similar to the charge/discharge behaviors of supercapacitor electrodes. As shown in the TEM results (Fig. 1), the average particle size of $NiFe_2O_4$ in the nanocomposite is much smaller than that of the pure $NiFe_2O_4$, which indicates that more lithium can be stored on the surface rather than in the bulk of the $NiFe_2O_4$ nanoparticles in the nanocomposite, leading to a shorter voltage plateau and a longer sloppy part for the charge/discharge curves. In addition, not only $NiFe_2O_4$ but also graphene can contribute to the lithium storage capacity. For the pure graphene electrode in this

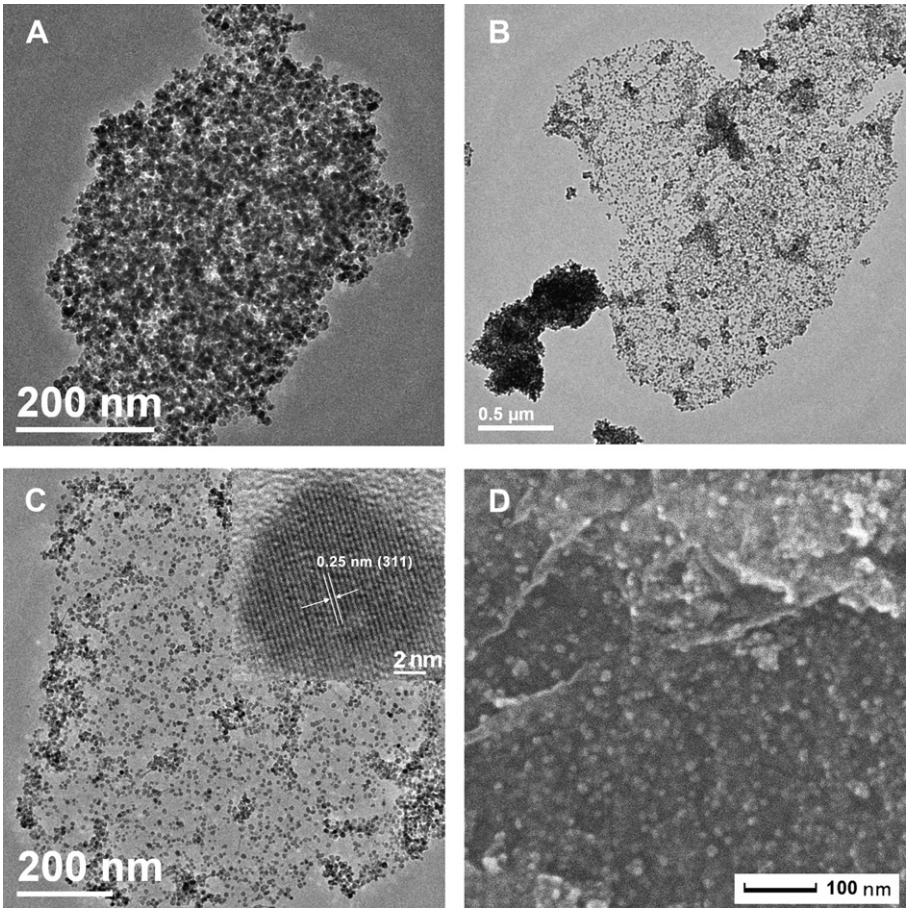

Fig. 1. TEM image of (A) pure $NiFe_2O_4$; (B) $NiFe_2O_4$–G(0.1); and (C, D) TEM and FESEM images of $NiFe_2O_4$–G(0.2) heteroarchitectures. The inset is high-resolution TEM image of $NiFe_2O_4$ nanoparticle lying on graphene sheet.

study, although the discharge and charge capacities for the first cycle are 1200 and 426 mAh g^{-1}, respectively (Fig. 2B), the capacities can be greatly enhanced in the case of exfoliated graphene sheets. As reported by Lian and Wang et al., the exfoliated graphene sheets with a curled morphology can deliver a discharge capacity of about 2035 mAh g^{-1} and a charge capacity of about 1264 mAh g^{-1} for the first cycle [20]. Therefore, the large specific surface area and the interfacial lithium storage mechanism of the $NiFe_2O_4$–graphene nanocomposite electrode could explain the shortened voltage plateau in the discharge curve and its large reversible capacity.

Fig. 2E shows the CV curves of the as-prepared $NiFe_2O_4$–G(0.2) nanocomposite and the pure $NiFe_2O_4$ electrodes at the 1st, 2nd, 5th, and 10th cycles at a scan rate of 1 mV s^{-1} between 0.01 and 3.00 V (vs. Li/Li^+). In the first cycle, cathodic peaks can be clearly observed at 0.44 V for the $NiFe_2O_4$–G(0.2) nanocomposite electrode and at 0.36 V for the pure $NiFe_2O_4$ electrode, which can be attributed to the reduction of Ni^{2+}/Fe^{3+} to Ni^0/Fe^0. In the reversible process, the anodic peaks at 1.78 V for the $NiFe_2O_4$–G(0.2) nanocomposite electrode and at 1.82 V for pure $NiFe_2O_4$ electrode could be ascribed to the oxidation of Ni^0/Fe^0 to Ni^{2+}/Fe^{3+}. The electrochemical reversible reaction can be expressed as

$$NiFe_2O_4 + 8e^- + 8Li^+ \Leftrightarrow Ni^0 + 2Fe^0 + 4Li_2O$$

In the subsequent cycles, the cathodic peak positively shifts to about 0.61 V while the anodic peak positively shifts to about 1.91 V for both the $NiFe_2O_4$–G(0.2) nanocomposite and the pure $NiFe_2O_4$ electrodes. Meanwhile, the CV curves of the $NiFe_2O_4$–G(0.2) nanocomposite electrode after the first cycle almost completely overlap, revealing improved cycling stability compared with the pure $NiFe_2O_4$ electrode, which matches well with the result of the discharge/charge measurements.

As shown in Fig. 2F, the pure $NiFe_2O_4$ electrode exhibits poor cycle performance and its capacity rapidly fades with cycling. After 50 cycles, the pure $NiFe_2O_4$ can deliver a reversible capacity of about 118 mAh g^{-1}, which is only 17% of that of the first cycle. When $NiFe_2O_4$–G contains 10 wt% graphene, 46% of the reversible capacity can be maintained over 50 cycles. The cycle performance can be further improved when the content of graphene is increased to 20 wt% in nanocomposite. After 50 cycles, the $NiFe_2O_4$–G(0.2) electrode delivers a reversible capacity of about 812 mAh g^{-1}, which is 85% of that of the first cycle. The $NiFe_2O_4$–G(0.2) electrode also exhibits excellent rate performance (Fig. 3A and B). At a high current density of 1000 mA g^{-1}, the $NiFe_2O_4$–G(0.2) electrode can still deliver a reversible capacity of about 445 mAh g^{-1}, which is much higher than that of the pure $NiFe_2O_4$ or $NiFe_2O_4$–G(0.1) electrode.

The superior electrochemical performance of the $NiFe_2O_4$–graphene nanocomposite can be attributed to its unique heteroarchitecture. In the $NiFe_2O_4$–G(0.2), $NiFe_2O_4$ nanoparticles are well-dispersed and anchored on graphene sheets, therefore the heteroarchitecture can provide a high electrode/electrolyte interface area and more lithium insertion/extraction sites, facilitating fast charge transfer between the active material and the electrolyte [17]. In the case of pure $NiFe_2O_4$, the nanoparticles may aggregate into

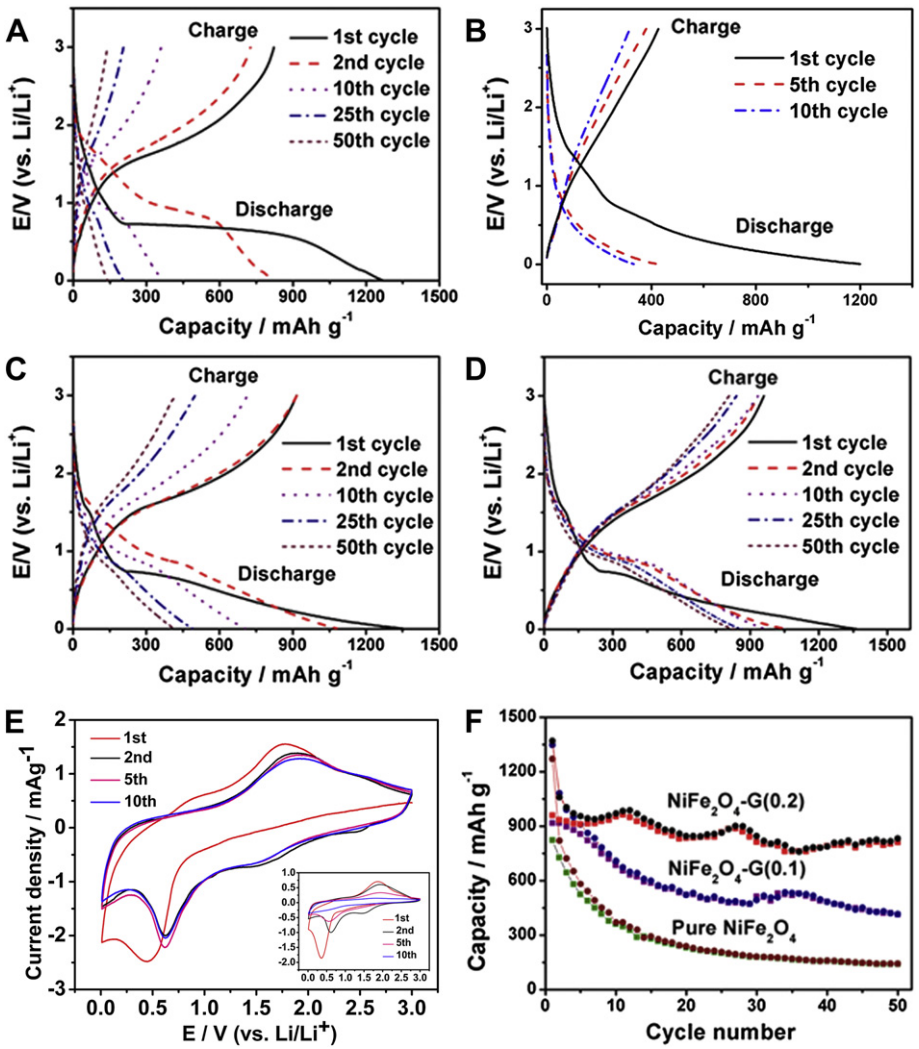

Fig. 2. Charge/discharge curves of (A) pure $NiFe_2O_4$, (B) reduced graphene oxide, (C) $NiFe_2O_4$–G(0.1), and (D) $NiFe_2O_4$–G(0.2) between 0.01 and 3 V at a current density of 100 mA g^{-1}. (E) Cyclic voltammograms of the $NiFe_2O_4$–G(0.2) and pure $NiFe_2O_4$ (the inset) at a scanning rate of 1 mV s^{-1}; and (F) comparison of cycle performance of pure $NiFe_2O_4$, $NiFe_2O_4$–G(0.1), and $NiFe_2O_4$–G(0.2).

several hundred nanometer clusters with reduced interface area, which block the penetration of electrolyte. These clusters could be pulverized due to the high strain induced during the charge/discharge processes and cause the loss of electrical contact between $NiFe_2O_4$ nanoparticles and current collector, thus leading to a degradation of capacity. Because the intimate interactions between the graphene substrates and the nanoparticles grown atop, the graphene sheets not only provide an elastic buffer space to accommodate the volume expansion/contraction of $NiFe_2O_4$ nanoparticles but also efficiently prevent the aggregation of $NiFe_2O_4$ nanoparticles. Single $NiFe_2O_4$ nanoparticle itself can accommodate big strain during charge/discharge due to its small particle size, which efficiently prevents the aggregation and cracking or crumbling of the electrode material upon cycling, and thus retains the

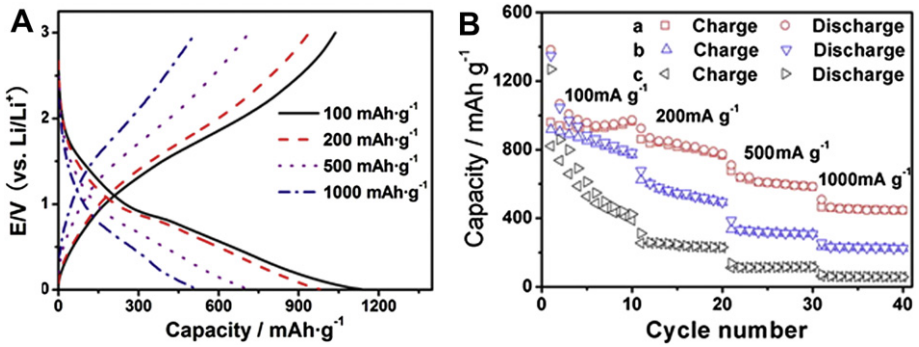

Fig. 3. (A) Charge/discharge curves of $NiFe_2O_4$–G(0.2) at different current densities. (B) Comparison of rate performance of (a) $NiFe_2O_4$–G(0.2), (b) $NiFe_2O_4$–G(10), and (c) $NiFe_2O_4$.

large capacity and excellent cycling stability. The good electrical conductivity of graphene sheets in $NiFe_2O_4$–graphene makes $NiFe_2O_4$ nanoparticles electrochemically active since charge carriers could be effectively and rapidly conducted back and forth from the $NiFe_2O_4$ nanoparticles to the current collector through the highly conducting three-dimensional graphene network, thus leading to high rate capability of the nanocompoiste electrode.

4. Conclusions

In summary, a $NiFe_2O_4$–graphene heteroarchitecture with well-dispersed $NiFe_2O_4$ nanoparticles has been fabricated by a hydrothermal method. Increasing the graphene content up to 20% in the nanocomposite can effectively prevent the aggregation of $NiFe_2O_4$ nanoparticles and significantly improve the electrochemical performance. $NiFe_2O_4$–G(0.2) exhibits a large reversible capacity about 960 mAh g^{-1} for the first cycle at a current density of 100 mA g^{-1}. It also exhibits excellent cycling stability and rate capability. The superior electrochemical performance of the $NiFe_2O_4$–graphene nanocomposite can be attributed to its unique heteroarchitecture, which enables high utilization of active material, good structural stability and fast charge transport.

Acknowledgments

This investigation was supported by NNSF of China (No. 21171094, 51102134), DFSR (No. A2620110010), PAPD of Jiangsu, NUST Research Funding (2011PYXM03, 2011ZDJH21) and the Department of Education of Jiangsu Province (CXZZ11_0245).

References

[1] P. Poizot, S. Laruelle, S. Grugeon, L. Dupont, J.M. Tarascon, Nature 407 (2000) 496.
[2] C.H. Jiang, E. Hosono, H.S. Zhou, Nano Today 1 (2006) 28.
[3] L.J. Zhi, Y.S. Hu, B.E. Hamaoui, X. Wang, I. Lieberwirth, U. Kolb, J. Maier, K. Mllen, Adv. Mater. 20 (2008) 1727.
[4] H. Xia, M.O. Lai, L. Lu, J. Mater. Chem. 20 (2010) 6896.
[5] Y. Wang, H.J. Zhang, J. Wei, C.C. Wong, J.Y. Lin, A. Borgna, Energy Environ. Sci. 4 (2011) 1845.
[6] Z.Y. Wang, D.Y. Luan, S. Madhavi, C.M. Li, X.W. Lou, Chem. Commun. 47 (2011) 8061.
[7] Y. Deng, Q. Zhang, S. Tang, L. Zhang, S. Deng, Z. Shi, G. Chen, Chem. Commun. 47 (2011) 6828.
[8] D.S. Wang, T. Xie, Q. Peng, S.Y. Zhang, J. Chen, Y.D. Li, Chem. Eur. J. 14 (2008) 2507.
[9] X.H. Huang, J.P. Tu, C.Q. Zhang, F. Zhou, Electrochim. Acta 55 (2010) 8987.
[10] L. Liu, S.M. Yuan, M. Ge, M.M. Ren, C.S. Sun, Z.J. Zhou, J. Phys. Chem. C 114 (2010) 251.
[11] X. Wang, L.J. Yu, X.L. Wu, F.L. Yuan, Y.G. Guo, Y. Ma, J.N.A. Yao, J. Phys. Chem. C 113 (2009) 15553.
[12] E. Yoo, J. Kim, E. Hosono, H. Zhou, T. Kudo, Nano Lett. 8 (2008) 2277.
[13] P. Lavela, J.L. Tirado, J. Power Sources 172 (2007) 379.
[14] H.X. Zhao, Z. Zheng, K.W. Wong, S. Wang, B.J. Huang, D.P. Li, Electrochem. Commun. 9 (2007) 2606.
[15] C.V. Abarca, P. Lavela, J.L. Tirado, J. Phys. Chem. C 114 (2010) 12828.
[16] Y.G. Guo, J.S. Hu, L.J. Wan, Adv. Mater. 20 (2008) 2878.
[17] J. Li, H. Dahn, L.J. Krause, D. Le, J.R. Dahn, J. Electrochem. Soc. 155 (2008) A812.
[18] S. Jin, H. Deng, D. Long, X. Liu, L. Zhan, X. Liang, W. Qiao, L. Ling, J. Power Sources 196 (2011) 3887.
[19] Y.S. Fu, H.Q. Chen, X.Q. Sun, X. Wang, AIChE J. (2011). doi:10.1002/aic.13716.
[20] P. Lian, X. Zhu, S. Liang, Z. Li, W. Yang, H. Wang, Electrochim. Acta 55 (2009) 3909.